FIRENZE 1991

ANALYSIS OF A SERIES–PARALLEL–LOADED RESONANT–CONVERTER WITH 'TERTIARY SIDE RESONANCE' FOR HIGH OUTPUT POWER AND LOW OUTPUT VOLTAGE

H.–P. Lüdeke, N. Fröhleke, H. Grotstollen
Institute for power electronics and electrical drives
University of Paderborn, Pohlweg 47–49, D–4790 Paderborn
Phone: 05251–603155 Fax: 05251–603238

Abstract. A series–parallel–loaded resonant–converter operating above resonance is proposed where the parallel tank capacitor is connected to the resonant circuit through a tertiary transformer winding. Thereby a part of the leakage inductance of the transformer is utilized as resonant element and by proper choice of the transformer ratio the ac–current in the parallel tank capacitor and the capacitor volume is reduced. General solutions for the state variables, converter gain, and component stress are obtained by an analysis in the time domain for steady-state operation including effects of the high-frequency transformer.

Keywords. Resonant–Converter, Component Stress, Operation above Resonance

INTRODUCTION

A common way to reduce the size of switch–mode power–supplies and to improve the transient response is to increase the switching frequency f_S. Because of the increasing switching losses with raised f_S in today used PWM–converters resonant converters have become interesting again. It has been shown by Steigerwald (1988) and Kunze (1989) that the series–parallel–loaded resonant–converter, known as SPRC or LCC-type parallel converter, operating above resonant frequency f_0, i.e. $f_S > f_0$, has many desirable features such as lossless switching with capacitive snubbers leading to excellent efficiency characteristics and low frequency range with wide input voltage and load range. For low output voltage and high output power applications it is not possible to utilize the leakage inductance of the transformer as resonant element by placing the parallel tank capacitor C_P on the secondary side of the transformer because C_P would have to carry an ac-current too high.
With the converter proposed in this paper it is possible to overcome these drawbacks. Here C_P is connected to the resonant circuit through a tertiary transformer winding – that's why the converter is called "SPRC with tertiary side resonance" (SPRCT). By proper choice of the primary to tertiary transformer ratio n_{13} the tertiary ac-current is reduced in order to use capacitors for higher voltages with ordinary rms–current ratings. Thus a technological solution results which is free of costly and high stressed components and makes use of parasitics, i.e. the leakage inductances of the transformer.

OPERATION OF A SPRCT ABOVE RESONANCE AND MODELLING

Figure 1 shows the circuit diagram of a half-bridge series-parallel-loaded resonant-converter with tertiary-side resonance. The switches S1 and S2, consisting of transistor T1 (T2) and antiparallel diode D1 (D2) (discrete or parasitic as for MOSFETs), operate in push-pull action. The capacitors C_1 and C_2 form the series-resonant capacitor of value $C_S = C_1 + C_2 = 2C_1$, the inductor L_r together with the primary and tertiary transformer leakage inductances $L_{\sigma 1}$ and $L_{\sigma 3}$ the resonant inductor. The voltage across the secondary transformer winding is rectified by D_3 to D_6 and smoothed by a L-C output filter (L_f, C_f). It has been found that the converter operates in two different modes. Referring to figures 1, 2 and 3a operation in *Mode 1* can be described as follows. The switching period starts with the turn-off of transistor T1. The voltage across C_P is positive and diodes D_3 and D_6 are conducting. The inductor current i_L changes from S1 to S2 (first to D_2 and at zero-crossing to T2). L_1 and L_3 resonate with C_P and C_S. When the input voltage of the bridge rectifier, i.e. the inverter output voltage, u_{12}, reaches zero output current I_a commutates from D_3, D_6 to D_4, D_5. u_{12} is clamped to zero during the commutation interval until i_2, the current in the secondary transformer winding, has reversed from $+I_a$ to $-I_a$. A resonant interval simi lar to the first one follows where the output current sink has changed its direction, see figure 2c. At half of the switching period, i.e. at $t = T_S/2$, transistor T2 is turned-off and in the second half of the switching period the operation described above repeats with S1 conducting.
For lighter loads and higher switching frequencies the converter enters into *Mode 2*. In this case the transistor is turned-off while the commutation of the output current has not finished. Therefore the commutation interval is devided into two intervals. A switching period starts with a *commutation interval*, is followed by the *energy-transfer interval* and then by a *commutation interval* as can be seen in figure 3c.

ANALYSIS

Assumptions

The analysis has been performed with the following assumptions:

- The switches, diodes and resonant elements are supposed to be ideal.

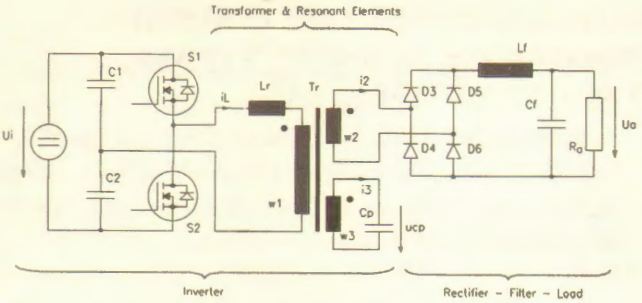

Fig. 1 Circuit diagram of a half-bridge series-parallel-loaded resonant-converter with tertiary side resonance

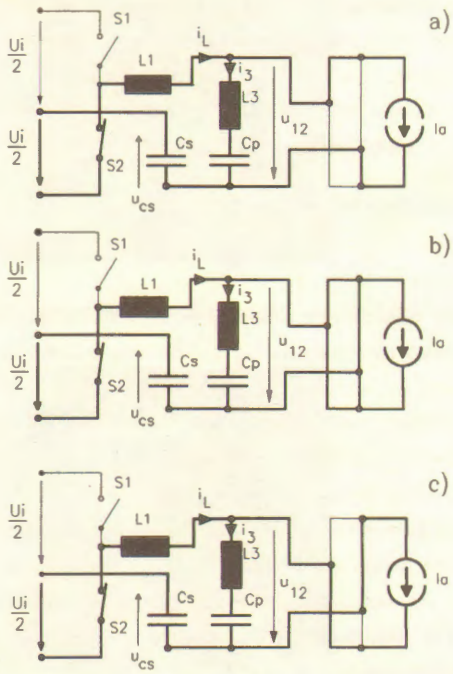

$$L_1 = L_r + L_{\sigma 1} \; ; \; L_3 = L_{\sigma 3} \tag{1}$$

Fig. 2 Equivalent circuit diagrams of the SPRCT
(Active branches marked by bold face lines)
a) *energy-return/transfer interval* $[\omega' t_0, \omega' t_1]$
b) *commutation-interval* $[\omega' t_1, \omega' t_2]$
c) *energy-transfer interval* $[\omega' t_2, \omega' t_3]$

- Input filter capacitor and output filter inductor are large enough to assume constant input voltage U_i and ripplefree output current I_a. The output filter together with the load can be treated as a constant-current sink.
- The effects of the snubber capacitors across the switches S1 and S2 are neglected.
- The three-winding-transformer is represented by a 'T'-equivalent circuit (presented e.g. by Middlebrook and Cuk (1981)) where the primary and tertiary leakage inductances are considered. The secondary leakage inductance can not be utilized as a resonant element and must be minimized at transformer realization. Therefore it is assumed to be zero. Fourth order differential equations would result, if $L_{\sigma 3}$ is taken into account.

General solutions

The analysis reveals that a switching period can be devided into six intervals with three intervals being sufficient to describe the behaviour of the converter mathematically because of symmetry between first and second halfperiod.

Node and mesh analysis of the equivalent circuits shown in figure 2 for the three intervals leads to the following equations for the four state variables i_L, current in the resonant inductor, i_3, current in the tertiary winding, u_{CS}, voltage at the series-resonant capacitor and u_{CP}, voltage at the parallel-resonant capacitor. Because of the neglected secondary leakage inductance ($L_{\sigma 2} = 0$) only differential equations of maximum order two appear.

Energy-return/transfer interval:

$$\frac{d^2}{dt^2} i_L(t) + \frac{C_S + C_P}{C_S \cdot C_P} \frac{1}{L_{13}} i_L(t) = \frac{1}{C_P L_{13}} I_a \tag{2}$$

$$i_3(t) = i_L(t) - I_a \tag{3}$$

$$u_{CP}(t) = \frac{1}{C_P} \cdot \int i_3(\tau)\, d\tau \tag{4}$$

$$u_{CS}(t) = \frac{1}{C_S} \cdot \int i_L(\tau)\, d\tau \tag{5}$$

Commutation-interval:

$$\frac{d^2}{dt^2} i_L(t) + \frac{1}{L_1 C_S} i_L(t) = 0 \tag{6}$$

$$\frac{d^2}{dt^2} i_3(t) + \frac{1}{L_3 C_P} i_3(t) = 0 \tag{7}$$

$$u_{CP}(t) = \frac{1}{C_P} \cdot \int i_3(\tau)\, d\tau \tag{8}$$

$$u_{CS}(t) = \frac{1}{C_S} \cdot \int i_L(\tau)\, d\tau \tag{9}$$

Energy-transfer interval:

$$\frac{d^2}{dt^2} i_L(t) + \frac{C_S + C_P}{C_S \cdot C_P} \frac{1}{L_{13}} i_L(t) = -\frac{1}{C_P L_{13}} I_a \tag{10}$$

$$i_3(t) = i_L(t) + I_a \tag{11}$$

$$u_{CP}(t) = \frac{1}{C_P} \cdot \int i_3(\tau)\, d\tau \tag{12}$$

$$u_{CS}(t) = \frac{1}{C_S} \cdot \int i_L(\tau)\, d\tau \tag{13}$$

Solving these equations leads to nonlinear equations for the state variables for each interval, containing the initial values i_{Li}, i_{3i}, u_{CSi}, u_{CPi}, the interval durations θ_i (with $i = 0, 1, 2$), and the load current as unknowns. For steady-state the values of the state variables at the end of the third interval, i.e. at $t = t_3 = T_S/2$, can be expressed by the initial values of the first interval using the condition that they are of the same amount but of different sign (because of symmetry between first and second halfperiod).

The average output voltage, important for calculating converter gain, can be derived from the rectified inverter output voltage $u_{12}(t)$, i.e. $U_a = \overline{u_a(t)} = \overline{|u_{12}(t)|}$. All equations are normalized using the following base quantities:

$$U_B = U_i \quad ; \quad I_B = \frac{U_B}{Z_B} \quad \text{with} \quad Z_B = \sqrt{\frac{L_1 + L_3}{C_S}} = \sqrt{\frac{L_{13}}{C_S}}.$$

An equation system with thirteen equations for Mode 1 and fourteen equations for Mode 2 follows which was solved numerically.

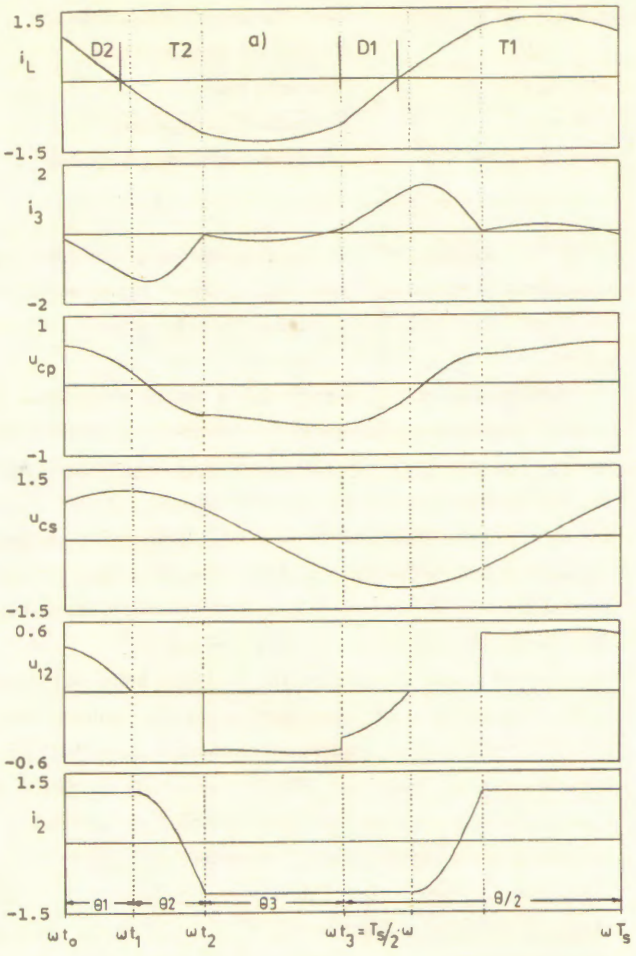

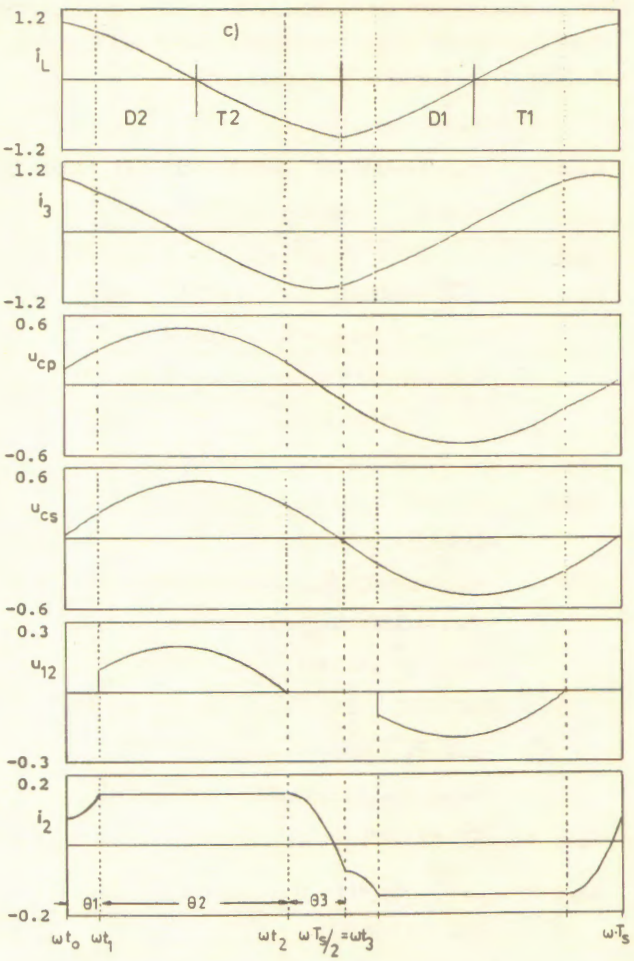

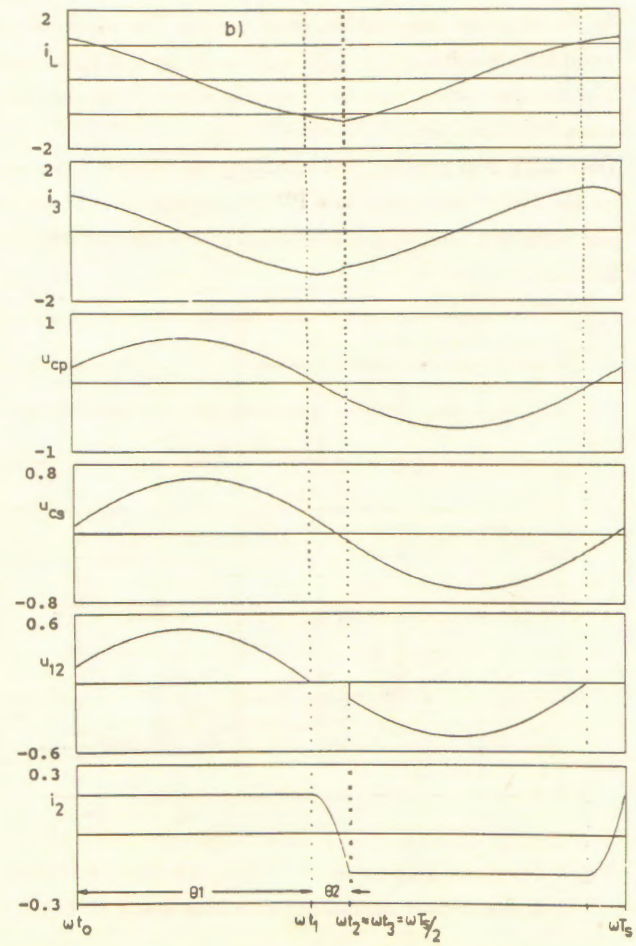

Fig. 3 Typical calculated waveforms of a SPRCT for

a) *Mode 1*: $\alpha = 1.0$, $\beta = 0.9$, $Q = 3.5$, $f_n = 1.307$, $M = 0.31$

b) *Boundary between Mode 1 and Mode 2*: $\alpha = 1.0, \beta = 0.9$, $Q = 0.6$, $f_n = 1.725$, $M = 0.282$

c) *Mode 2*: $\alpha = 1.0$, $\beta = 0.8$, $Q = 1.5$, $f_n = 1.813$, $M = 0.097$

The equation system for Mode 1 is given below as an example where the subscript 'n' marks normalized values and the subscript '0', '1' or '2' the border of an interval looked at.

$$
\begin{aligned}
u_{cpn0} &= -(i_{Ln2}D + QMAD)\cdot\sin(\theta 3) + QM\cdot\theta 3\cdot(AD-D) \\
&\quad -u_{cpn2} + A\cdot(u_{c2n2}+u_{cpn2})\cdot[1-\cos(\theta 3)] \\
u_{cpn2} &= (i_{Ln1}-QM)\cdot\frac{1}{H}\cdot\sin(\gamma\theta 2) + u_{cpn1}\cdot\cos(\gamma\theta 2) \\
u_{cpn1} &= (i_{Ln0}D - QMAD)\cdot\sin(\theta 1) + QM\cdot\theta 1\cdot(AD-D) \\
&\quad + u_{cpn0} + A\cdot(u_{c2n0}+u_{cpn0})\cdot[\cos(\theta 1)-1] \\
i_{Ln0} &= -i_{Ln2}\cdot\cos(\theta 3) + (u_{c2n2}+u_{cpn2})\cdot E\cdot\sin(\theta 3) \\
&\quad + QMA[1-\cos(\theta 3)] \\
i_{Ln2} &= i_{Ln1}\cdot\cos(\rho\theta 2) - u_{c2n1}\cdot G\cdot\sin(\rho\theta 2) \\
i_{Ln1} &= i_{Ln0}\cdot\cos(\theta 1) - (u_{c2n0}+u_{cpn0})\cdot E\cdot\sin(\theta 1) \\
&\quad + QMA[1-\cos(\theta 1)] \\
QM &= -i_{Ln1}\cdot\cos(\rho\theta 2) + u_{c2n1}\cdot G\cdot\sin(\rho\theta 2) \\
&\quad + (i_{Ln1}-QM)\cdot\cos(\gamma\theta 2) \\
&\quad - u_{cpn1}\cdot H\cdot\sin(\gamma\theta 2) \\
0 &= [QM\cdot(DC-AD) + i_{Ln0}\cdot(D-F)]\cdot\sin(\theta 1) \\
&\quad + QM\cdot\theta 1\cdot(AD-D) + u_{cpn0} \\
&\quad + (u_{c2n0}+u_{cpn0})\cdot[\cos(\theta 1)\cdot(A-C)-A] \\
u_{c2n2} &= \frac{i_{Ln1}}{G}\cdot\sin(\rho\theta 2) + u_{c2n1}\cdot\cos(\rho\theta 2) \\
u_{c2n1} &= i_{Ln0}\cdot\frac{B}{E}\cdot\sin(\theta 1) + B\cdot(u_{c2n0}+u_{cpn0})\cdot\cos(\theta 1) \\
&\quad - QMBD\cdot\sin(\theta 1) \\
u_{c2n0} &= \left[QM(AD-DC-BD) + i_{Ln2}\left(D-F-\frac{B}{E}\right)\right]\sin(\theta 3) \\
&\quad + (u_{c2n2}+u_{cpn2})\cdot[\cos(\theta 3)\cdot(A-C-B)-A] \\
&\quad + u_{cpn2} - QM\cdot\theta 3\cdot(AD-D) + 1 \\
M\cdot\frac{\theta}{2} &= [QM\cdot(CD-AD) + i_{Ln0}\cdot(D-F)]\cdot[1-\cos(\theta 1)] \\
&\quad + \frac{QM\cdot\theta 1^2}{2}\cdot(AD-D) + u_{cpn0}\cdot\theta 1 \\
&\quad + (u_{cpn0}+u_{c2n0})\cdot[\sin(\theta 1)\cdot(A-C) - A\cdot\theta 1] \\
&\quad + [QM\cdot(CD-AD) + i_{Ln2}\cdot(D-F)]\cdot[1-\cos(\theta 3)] \\
&\quad + \frac{QM\cdot\theta 3^2}{2}\cdot(AD-D) - u_{cpn2}\cdot\theta 3 \\
&\quad - (u_{cpn2}+u_{c2n2})\cdot[\sin(\theta 3)\cdot(A-C) - A\cdot\theta 3] \\
\theta &= 2\cdot(\theta 1+\theta 2+\theta 3) \qquad (14)
\end{aligned}
$$

with:

$$A=\tfrac{1}{1+\alpha} \qquad B \stackrel{!}{=} \beta = \tfrac{L_1}{L_{13}} \qquad C=\tfrac{L_3}{L_{13}} \qquad D=\sqrt{\tfrac{1+\alpha}{\alpha}}\cdot A$$

$$E=\sqrt{\tfrac{\alpha}{1+\alpha}} \qquad F=\sqrt{\tfrac{1+\alpha}{\alpha}}\cdot C \qquad G=\sqrt{\tfrac{1}{B}} \qquad H=\sqrt{\tfrac{\alpha}{C}}$$

$$\rho = E\cdot G \qquad \gamma=\sqrt{\tfrac{1}{1+\alpha}\cdot\tfrac{1}{C}}$$

$$u_{c2n} = u_{csn} + 0.5$$

$\alpha = C_P/C_S$	Capacitance ratio
$\beta = L_1/L_{13}$	Inductance ratio
$\theta_1, \theta_2, \theta_3$	Duration of intervals ($\theta_i = \omega'(t_i - t_{i-1})$)
$\theta = \omega' T_S$	Duration of a switching period
$\omega' = \omega\cdot\sqrt{(1+\alpha)/\alpha}$	Converter resonant frequency
$\omega = \sqrt{L_{13}C_S}^{-1}$	Resonant frequency
$Z = \sqrt{L_{13}/C_S}$	Characteristic circuit impedance
$Q = Z/R_a$	Normalized load resistance
$M = U_a/U_i$	Converter gain
$QM = I_{an}$	Normalized load current
$f_n = 2\pi\cdot f_s/\omega$	Normalized switching frequency

With the solutions given above, (14), operating waveforms and converter gain can be obtained. Figure 3 shows typical waveforms for Mode 1 and Mode 2 in normalized form for a whole switching period.

The border of an interval is marked by a dotted vertical line. Figure 3b shows the waveforms at the boundary between the two modes. The duration of the third interval (*energy-transfer interval*) has become zero and the converter behaviour is described by the *energy-return/transfer interval* and the *commutation-interval*

Figures 4 to 6 show operation diagrams – converter gain M versus normalized switching frequency f_n with normalized load resistance Q as parameter – for different values of α and β.

Variation of α and β influences the converter behaviour significantly. Increasing α, i.e. enlarging the parallel-resonant capacitance C_P, let the series-parallel-loaded resonant-converter (SPRC) become a parallel-loaded one (PRC). Accordingly the SPRC becomes a series-loaded resonant-converter (SRC) by decreasing α, i.e. enlarging the series-resonant capacitance C_S.

β describes the distribution of the resonant inductance to the primary and tertiary transformer side. Concentrating the whole resonant inductance on the primary side, corresponding to $\beta = 1.0$, represents the ideal SPRC without leakage inductances analyzed by Kunze in the time and frequency domain. The operation diagram for $\alpha = 1.0$ and $\beta = 0.999$ is given in figure 4 (solid lines). The diamonds and X represent operating points of the ideal SPRC taken from the operation diagram of Kunze.

Decreasing β to zero, i.e. concentrating the resonant inductance on the tertiary side, leads to a PWM-converter between primary and secondary side additionally loaded with a resonant circuit on the tertiary side.

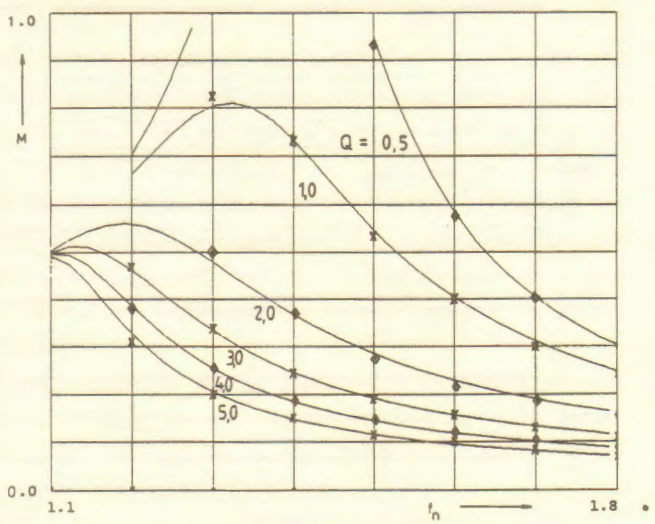

Fig. 4 Operation diagram for $\alpha = 1.0$, $\beta = 0.999$ (solid lines). X and ◇ mark operating points from Kunze (1989)

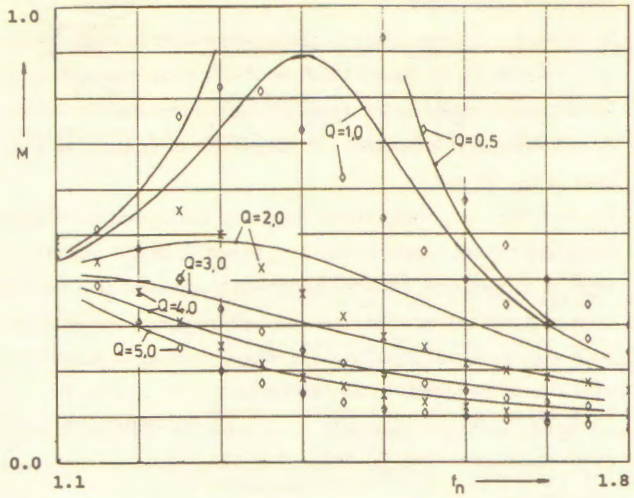

Fig. 5 Comparison of operation diagrams for $\alpha = 1.0$, $\beta = 0.9$ (solid lines) and $\alpha = 1.0$, $\beta = 0.999$ (X and ◇) ($\hat{=}$ ideal SPRC)

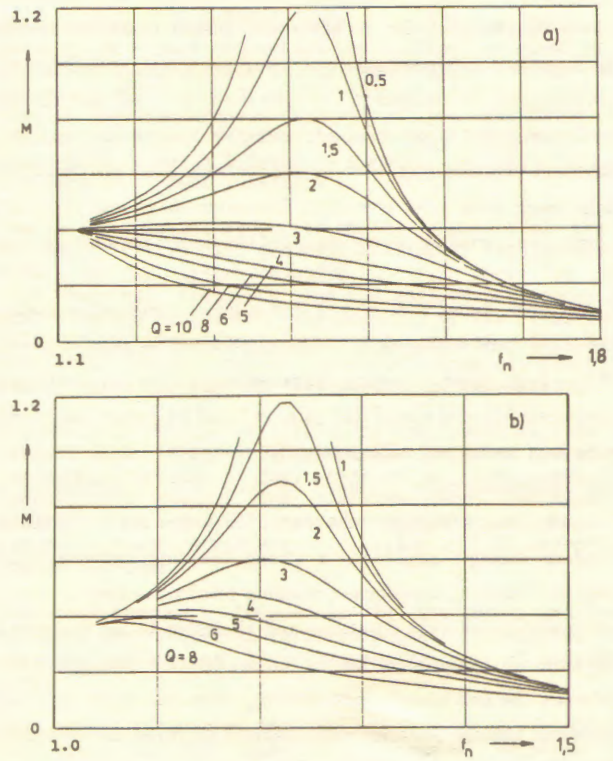

Fig. 6 Operation diagrams for $\alpha = 1.0$, $\beta = 0.8$ (a) and $\alpha = 2.0, \beta = 0.9$ (b)

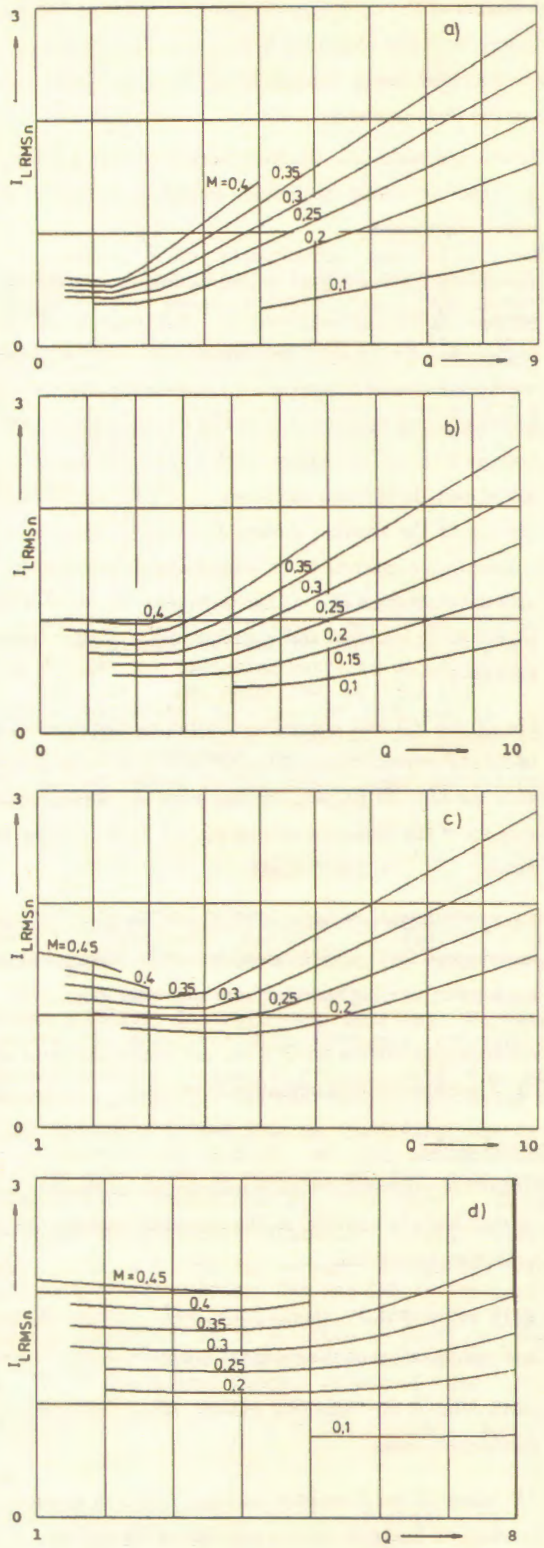

Fig. 7 Stress diagrams for the RMS-value of the inductor current in normalized form.
a) $\alpha = 0.5$, $\beta = 0.9$, b) $\alpha = 1.0$, $\beta = 0.9$,
c) $\alpha = 1.0$, $\beta = 0.8$, d) $\alpha = 2.0$, $\beta = 0.9$,

The deviation of the operation diagrams considering the leakage inductances from the ideal case is shown in figure 5 for $\alpha = 1.0$ and $\beta = 0.9$ (solid lines). Diamonds and X again mark operating points of the ideal converter.

- In the non ideal case the maximum converter gain appears at higher switching frequencies caused by shifted converter input impedances.
- For $Q \geq\approx 2.0$ and higher switching frequencies the converter gain of the SPRC considering the leakage inductances is higher than for the ideal one. In the ideal case the capacitor voltage u_{CP} is the input voltage of the bridge rectifier. After a zero-crossing or at the end of the discontinuous-capacitor-voltage interval (see Kunze, 1989), u_{CP} increases in a sinusoidal way. In the non ideal case ($\beta < 1.0$), u_{12} is the input voltage of the rectifier diodes, jumping at the end of the commutation interval to an amplitude, determined by u_{CP} and the derivation of i_3 at this moment. Therefore a higher time-voltage product and consequently a higher converter gain results.
- For $Q \geq\approx 2.0$ and normalized switching frequencies closer to 1.0 the converter gain of the SPRCT is lower as compared with the ideal SPRC because the influence of the resonance step-up of the capacitor voltage u_{CP} at $f_S \approx f_0$ is less significant.
- For $Q \leq 1.0$ the minimum of the converter input impedance is decreased for the SPRC considering the leakage inductances leading to a higher maximum converter gain.

The converter gain curves for $Q \leq 0.5$ are nearly the same as for $Q = 0.5$. Therefore no-load operation is possible.

Component stress

To optimize the converter design knowledge about the component stress is essential. In addition to the maximum ratings the following quantities are useful:

- RMS value of the inductor current, I_{LRMS}, for the design and optimization of the resonant inductor,
- RMS value of the transistor current, I_{SRMS}, to estimate the conduction losses,
- AV value of the transistor current, I_{SAV}, to estimate the conduction losses, if bipolar transistors are applied,
- RMS value of the capacitor voltages, U_{CPRMS}, U_{CSRMS}, for selection of appropriate capacitors,
- time-voltage product at the transformer terminals for its design.

Equations for the desired AV- and RMS-values and the time-voltage product can be derived from the general solutions leading to stress diagrams (normalized RMS- or AV-value versus normalized load resistance with converter gain as parameter). Figure 7 shows the normalized RMS-value of the resonant-inductor current, I_{LRMSn}, for different values of α and β and typical load and converter gain ranges.

Increasing α leads to stress diagrams insensitive to load variations in a wide range, see figure 7d. A poor efficiency characteristic for lighter loads results as for a parallel-loaded resonant-converter.

A variation of β influences the magnitude of I_{LRMSn} as can be seen in fig. 7b and 7c.

Beyond the component stress diagrams the operation diagrams have to be taken into consideration to optimize the converter design. A compromise between minimum component stresses – leading to small values of α – and a small frequency range together with wide load and input voltage range – leading to larger values of α – must be found. In any case β should be close to 1.

To verify the theoretical results realization of a SPRC with tertiary side resonance is in preparation considering the above mentioned optimization hints.

CONCLUSIONS

The state variables waveforms, the converter gain and component stress diagrams of the series-parallel-loaded resonant-converter with tertiary side resonance operating above resonant frequency, derived from an analysis in the time domain reveal that the converter, utilizing a part of the transformer leakage inductances as resonant element, can be designed for wide load and input voltage range with a relative small frequency range and acceptable component stress by proper choice of the design parameters α and β.

It has been found that $\alpha \approx 1.0$ is a good compromise making use of the main advantages of the series-loaded resonant-converter (SRC) (e.g. good efficiency characteristic for lighter loads) and the parallel-loaded one (PRC) (e.g. reduced frequency range with wide load and input voltage range).

The inductance ratio β should be close to 1, corresponding to a small tertiary leakage inductance. Together with a small secondary leakage inductance a strong coupling between secondary and tertiary transformer winding results, leading to shorter commutation-interval durations and therefore to an increase of the time-voltage product for the output filter. A strong coupling between the two transformer windings does not make too much problems because isolation specifications need not to be considered. Thus, strong coupling leads to the projected reduction in blocking voltage of the rectifying power diodes on the secondary side which affects reduced conduction losses of the dominant loss generating components.

REFERENCES

1) **Kunze, J.** (1989). "Untersuchung ausgewählter Resonanz-Konverter für hohe Ausgangsleistung bei geringer Ausgangsspannung". M.S. Thesis, University of Paderborn.

2) **Middlebrook, R.D. and Cuk, S.** (1981). "Advances in switched mode power conversion, Volume I, Modelling, Analysis and Measurement, No. 13: Transformer modelling and design for leakage control". Teslaco, Pasadena, USA, pp. 205-218.

3) **Steigerwald, R.** (1988). "A comparison of half-bridge resonant converter topologies". IEEE Transactions on Power Electronics, PE 3, No 2, 174-182.